Oncogene (2014) **33,** 882–890

www.nature.com/onc

ORIGINAL ARTICLE

RNAi-mediated stathmin suppression reduces lung metastasis in an orthotopic neuroblastoma mouse model

FL Byrne[1], L Yang[1], PA Phillips[2], LM Hansford[3], JI Fletcher[4], CJ Ormandy[5], JA McCarroll[1,6] and M Kavallaris[1,6]

Metastatic neuroblastoma is an aggressive childhood cancer of neural crest origin. Stathmin, a microtubule destabilizing protein, is highly expressed in neuroblastoma although its functional role in this malignancy has not been addressed. Herein, we investigate stathmin's contribution to neuroblastoma tumor growth and metastasis. Small interfering RNA (siRNA)-mediated stathmin suppression in two independent neuroblastoma cell lines, BE(2)-C and SH-SY5Y, did not markedly influence cell proliferation, viability or anchorage-independent growth. In contrast, stathmin suppression significantly reduced cell migration and invasion in both the neuroblastoma cell lines. Stathmin suppression altered neuroblastoma cell morphology and this was associated with changes in the cytoskeleton, including increased tubulin polymer levels. Stathmin suppression also modulated phosphorylation of the actin-regulatory proteins, cofilin and myosin light chain (MLC). Treatment of stathmin-suppressed neuroblastoma cells with the ROCKI and ROCKII inhibitor, Y-27632, ablated MLC phosphorylation and returned the level of cofilin phosphorylation and cell invasion back to that of untreated control cells. ROCKII inhibition (H-1152) and siRNA suppression also reduced cofilin phosphorylation in stathmin-suppressed cells, indicating that ROCKII mediates stathmin's regulation of cofilin phosphorylation. This data demonstrates a link between stathmin and the regulation of cofilin and MLC phosphorylation via ROCK. To examine stathmin's role in neuroblastoma metastasis, stathmin short hairpin RNA (shRNA)\luciferase-expressing neuroblastoma cells were injected orthotopically into severe combined immunodeficiency-Beige mice, and tumor growth monitored by bioluminescent imaging. Stathmin suppression did not influence neuroblastoma cell engraftment or tumor growth. In contrast, stathmin suppression significantly reduced neuroblastoma lung metastases by 71% ($P<0.008$) compared with control. This is the first study to confirm a role for stathmin in hematogenous spread using a clinically relevant orthotopic cancer model, and has identified stathmin as an important contributor of cell invasion and metastasis in neuroblastoma.

Oncogene (2014) **33,** 882–890; doi:10.1038/onc.2013.11; published online 11 February 2013

Keywords: orthotopic xenograft; cytoskeleton; cofilin; tubulin

INTRODUCTION

Neuroblastoma is the most common extracranial solid tumor in children, accounting for 6–10% of all childhood cancers and 15% of all pediatric cancer deaths.[1] Neuroblastoma arises from precursor cells of the sympathetic nervous system, and metastases are found in ~50% of patients at diagnosis (reviewed in Ara and DeClerck[2]). Although neuroblastoma tumors are found throughout the body (bone marrow, bone, lymph nodes, liver, intracranial and orbital sites),[3] lung metastases indicate the most advanced disease and confer the worst prognosis (5-year overall survival rates of $34.5 \pm 6.8\%$ compared with $44.7 \pm 1.3\%$ for children with advanced-stage disease without lung metastasis).[4] Thus, metastatic tumors are the major cause of death for neuroblastoma patients though the mechanisms driving metastasis in this disease are not well characterized.

Metastasis is initiated when cancer cells leave the primary tumor and migrate and invade the surrounding extracellular matrix. Cues from the plasma membrane induce guanosine triphosphatase activation of the small Rho GTPases and various signaling pathways that lead to restructuring of the cell cytoskeleton (reviewed in Insall and Machesky[5]). Activation of the Rho–Rho associated coiled–coil forming protein serine/threonine kinase (Rho–ROCK) signaling pathway regulates remodeling of the actin network via the phosphorylation of cofilin and myosin light chain (MLC),[6] as well as microtubules.[7] Thus, this signaling pathway has an important role in cell migration and invasion.

Microtubules comprise of head-to-tail aligned α-tubulin and β-tubulin heterodimers that constantly switch between phases of growth (polymerization) and shrinking (depolymerization). This feature, termed 'dynamic instability', is regulated by various interacting proteins such as stathmin (*STMN1*). Stathmin, a ubiquitously-expressed cytosolic phosphoprotein, is the founding member of the highly homologous stathmin-like protein family that includes superior cervical ganglion-10 protein (*STMN2*), SCLIP (*STMN3*), RB3 (*STMN4*) and its splice variants RB3' and RB3''.[8] All stathmin-like proteins bind two α/β-tubulin heterodimers and function to destabilize the microtubules.[8] In many non-neuronal malignancies[9–13] and adult neuroendocrine tumors,[14] overexpression of stathmin correlates with metastatic disease and often confers a poor prognosis. Stathmin is also highly expressed

[1]Tumour Biology and Targeting Program, Children's Cancer Institute Australia, Lowy Cancer Research Centre, University of New South Wales, Randwick, New South Wales, Australia; [2]Pancreatic Cancer Translational Research Group, School of Medical Sciences, University of New South Wales, Randwick, New South Wales, Australia; [3]Cell Biology Program, Hospital for Sick Children, University of Toronto, Toronto, ON, Canada; [4]Experimental Therapeutics Program, Children's Cancer Institute Australia, Lowy Cancer Research Centre, University of New South Wales, Randwick, New South Wales, Australia; [5]Cancer Research Program, Garvan Institute of Medical Research, Darlinghurst, New South Wales, Australia and [6]Australian Centre for Nanomedicine, University of New South Wales, Randwick, New South Wales, Australia. Correspondence: Professor M Kavallaris or Dr JA McCarroll, Tumour Biology and Targeting Program, Children's Cancer Institute Australia, Lowy Cancer Research Centre, University of New South Wales, P.O. Box 81, Randwick, New South Wales 2031, Australia.
E-mail: mkavallaris@ccia.unsw.edu.au or jmccarroll@ccia.unsw.edu.au
Received 17 August 2012; revised 25 November 2012; accepted 3 December 2012; published online 11 February 2013

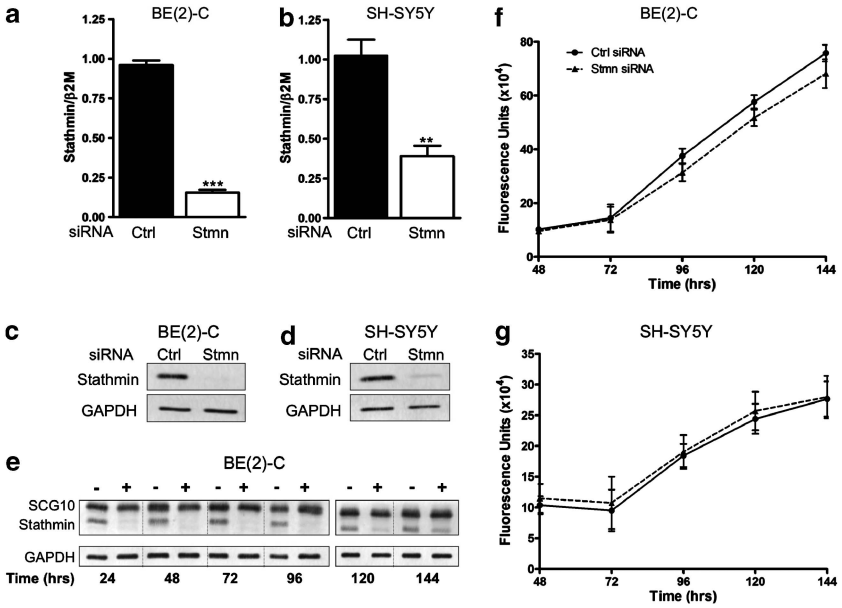

Figure 1. siRNA-mediated stathmin suppression does not influence neuroblastoma cell proliferation. Stathmin mRNA levels in BE(2)-C (**a**) and SH-SY5Y cells (**b**) 48 h post transfection with stathmin (Stmn) or control (Ctrl) siRNA. $^{**}P<0.005$, $^{***}P<0.001$. Representative western blots of stathmin protein expression in BE(2)-C (**c**) and SH-SY5Y cells (**d**) 72 h post transfection with Stmn or Ctrl siRNA. (**e**) Representative western blot of superior cervical ganglion-10 protein and stathmin protein expression in stathmin siRNA (+) or Ctrl siRNA (−) BE(2)-C cells 24–144 h after double siRNA transfection. Proliferation of BE(2)-C (**f**) and SH-SY5Y cells (**g**) transfected with Stmn or Ctrl siRNA.

in neuroblastoma tumors and cell lines[15,16] and is upregulated in vincristine-resistant neuroblastoma cells,[17] although its functional role in this aggressive malignancy has not been elucidated. In this study we used RNA interference to suppress stathmin expression and examine its role in neuroblastoma tumor growth and metastasis.

RESULTS

Small interfering RNA-mediated stathmin suppression in neuroblastoma cells

A gene silencing approach was used to investigate stathmin's functional role in neuroblastoma. Stathmin Smartpool small interfering RNA (siRNA) effectively suppressed stathmin mRNA (Figures 1a and b) and protein (Figures 1c and d) expression in two independent neuroblastoma cell lines, BE(2)-C and SH-SY5Y. Stathmin transcript levels were reduced by $83.9 \pm 1.77\%$ ($P<0.0001$) in BE(2)-C cells (Figure 1a) and $61.9 \pm 6.3\%$ ($P<0.005$) in SH-SY5Y cells compared with controls (Figure 1b). Double siRNA-transfection of BE(2)-C cells prolonged stathmin protein suppression up to 144 h (Figure 1e). Stathmin siRNA was specific as it did not induce any alterations in the expression of the highly homologous stathmin-like proteins superior cervical ganglion-10 protein (Figure 1e) or SCLIP (data not shown).

Stathmin does not regulate neuroblastoma cell proliferation, viability, cell cycle progression or anchorage-independent growth

Given stathmin's role as a microtubule regulating protein, we examined whether stathmin influenced proliferation of neuroblastoma cells. Stathmin suppression did not markedly affect BE(2)-C or SH-SY5Y cell proliferation (Figures 1f and g), and only a small decrease in the G_1 phase of the cell cycle was observed in stathmin-suppressed cells compared with controls ($61.91 \pm 0.42\%$ in stathmin siRNA-treated cells compared with $64.3 \pm 0.69\%$ in control cells; $P<0.05$) (Supplementary Figure S1A). Furthermore, only a minor decrease in cell viability was observed in stathmin-suppressed BE(2)-C cells at 48 h post siRNA transfection, an effect not seen at other time points (Supplementary Figure S1B).

We also determined whether stathmin influenced neuroblastoma anchorage-independent growth and found that stathmin suppression did not alter the ability of BE(2)-C (Supplementary Figure S1C) or SH-SY5Y cells (data not shown) to grow in soft agar. These results indicate that stathmin does not have a major role in regulating neuroblastoma cell proliferation or anchorage-independent growth.

Stathmin regulates chemotactic-induced neuroblastoma cell migration and invasion

To determine whether stathmin had a role in neuroblastoma cell migration and invasion, stathmin-suppressed cells were subjected to chemotaxis migration and invasion assays. Stathmin suppression significantly reduced the migratory ability of BE(2)-C cells by 47% (migration index of 3.06 ± 0.23 for stathmin siRNA-treated cells vs 5.81 ± 0.08 for control cells; $P<0.001$) (Figure 2a) and SH-SY5Y cells by 44% (migration index of 2.65 ± 0.25 for stathmin siRNA-treated cells vs 4.72 ± 0.65 for control cells; $P<0.05$) (Figure 2b). Moreover, stathmin suppression significantly inhibited the invasion of BE(2)-C cells through Matrigel by 62% (invasion index of 8.55 ± 2.16 for stathmin siRNA-treated cells vs 22.76 ± 3.54 for control cells; $P<0.05$) (Figure 2c) and SH-SY5Y cells by 56% (invasion index of 8.72 ± 1.64 for stathmin siRNA-treated cells vs 19.61 ± 2.48 for control cells; $P<0.05$) (Figure 2d). Collectively, these results demonstrate that stathmin has a role in chemotactic-induced neuroblastoma cell migration and invasion.

Stathmin suppression alters the cytoskeleton and morphology of neuroblastoma cells

In order to understand the potential mechanisms by which stathmin was mediating neuroblastoma cell migration and invasion, we examined the morphology and cytoskeleton of stathmin-suppressed BE(2)-C cells in both serum-free conditions (Figure 3) and growth factor-treated conditions (data not shown). In both conditions, similar alterations in cell morphology were observed. In particular, stathmin-suppressed cells displayed increased numbers of short and thin neurite-like extensions compared with controls (Figure 3a). Phalloidin staining confirmed

that these projections comprised of actin filaments (*white arrows*) (Figure 3b). Only a small change in microtubule density was observed between stathmin-suppressed cells and controls (Figure 3b, *inset image*).

To further examine stathmin's role in regulating the microtubule network in neuroblastoma cells, tubulin polymer levels were analyzed in siRNA-treated BE(2)-C cells (Figure 4a). Importantly, cells were cultured in conditions that mimicked those used for the cell migration and invasion assays (serum-starved and serum-starved plus growth factor treatment). Under both conditions, stathmin suppression increased tubulin polymer levels (an increase of 29% ($P<0.05$) in serum-starved conditions and 24% ($P=0.11$) in growth factor-treated conditions) compared with controls (Figure 4a). This data supports a role for stathmin in regulating tubulin polymer levels in neuroblastoma cells.

Given the changes in cell morphology and the increase in actin-rich projections from the cell bodies following stathmin suppression, we hypothesized that regulation of the actin cytoskeleton was altered. To address this, we examined the expression and phosphorylation of cofilin, a major regulator of the actin network,[18] in stathmin-suppressed BE(2)-C cells (Figure 4b). Interestingly, a clear increase in cofilin phosphorylation was observed in stathmin-suppressed cells in both serum-free and growth factor-treated conditions compared with controls (Figure 4b, arrows). In addition, increases in cofilin phosphorylation induced by stathmin suppression were maintained over time following growth factor treatment, compared with controls (Supplementary Figure S2A). Cofilin phosphorylation declined in controls 30 min post growth factor treatment, but was maintained up to 60 min post growth factor treatment in stathmin-suppressed cells (Supplementary Figures S2A and B). Total levels of cofilin were not altered. These results indicate that stathmin regulates cofilin phosphorylation in both serum-starved and growth factor-treated conditions in neuroblastoma cells.

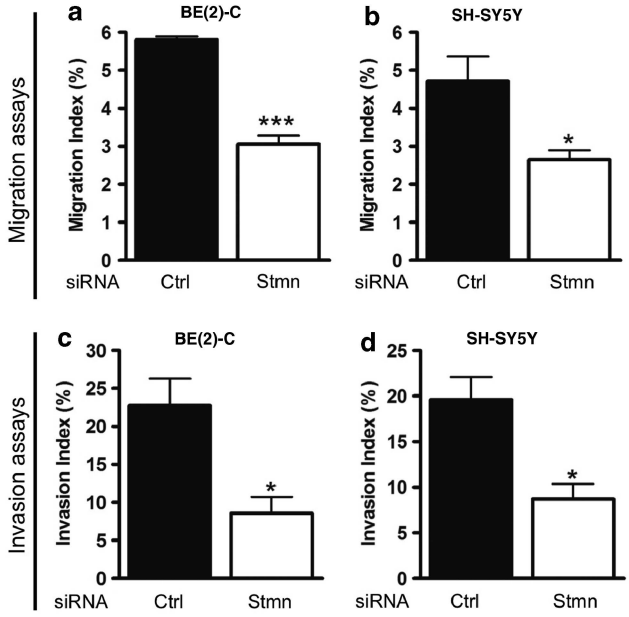

Figure 2. Stathmin regulates chemotactic-induced neuroblastoma cell migration and invasion. Chemotactic-induced migration of stathmin (Stmn) and control (Ctrl) siRNA-transfected BE(2)-C (**a**) and SH-SY5Y cells (**b**). Chemotactic-induced cell invasion of Stmn and Ctrl siRNA-transfected BE(2)-C (**c**) and SH-SY5Y cells (**d**). *$P<0.05$, ***$P<0.001$.

Stathmin suppression-induced increases in cofilin and MLC phosphorylation are reversed by treatment with a ROCK inhibitor

The Rho-ROCK signaling pathway and its downstream effector proteins are major regulators of the actin network during cell migration. Cofilin and MLC are phosphorylated upon activation of this signaling pathway.[19] In order to determine whether stathmin was regulating cofilin phosphorylation via ROCK, Y-27632, a compound that inhibits the kinase activity of p160ROCK (ROCKI) and ROKα/Rho-kinase (ROCKII), was used to block ROCK signaling.[20] siRNA-transfected BE(2)-C cells were treated with 10–40 μmol/l Y-27632 (concentrations that were not toxic to the cells, data not shown), which partially reduced cofilin phosphorylation in both control and stathmin-suppressed cells (Figure 4c). Notably, the levels of cofilin phosphorylation in stathmin-suppressed cells were returned to that of untreated control cells, an effect that was consistently observed irrespective of Y-27632 concentration (Figure 4c). This was further validated using H-1152, an inhibitor of ROCKII,[21] further confirming stathmin's regulation of cofilin phosphorylation via ROCK (Supplementary Figure S3A). Moreover, the suppression of ROCKII using siRNA also reduced cofilin phosphorylation in stathmin-suppressed cells back to that of control cells (Supplementary Figures S3C, D). Conversely,

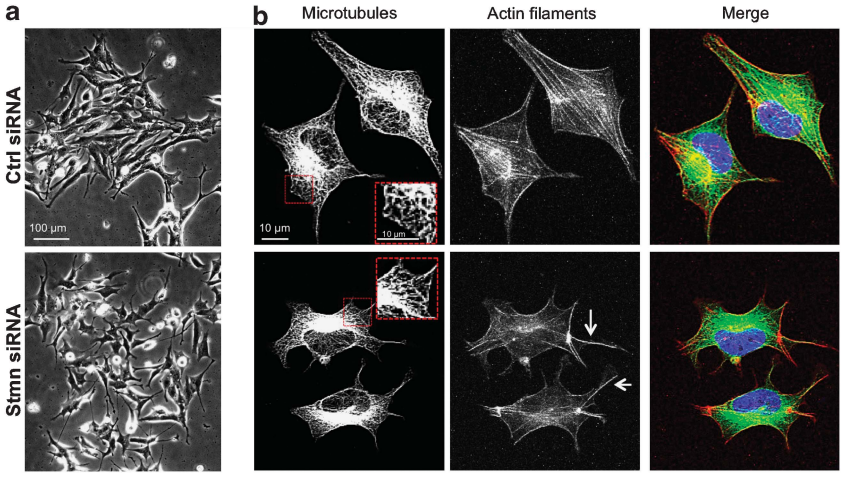

Figure 3. Stathmin regulates neuroblastoma cell morphology. (**a**) Phase-contrast images of control (Ctrl) and stathmin (Stmn) siRNA-treated BE(2)-C cells. (**b**) Black and white confocal images of actin filaments and microtubules in Ctrl and Stmn siRNA-treated BE(2)-C cells. The merged color image shows microtubules in green, actin filaments in red and nuclei in blue.

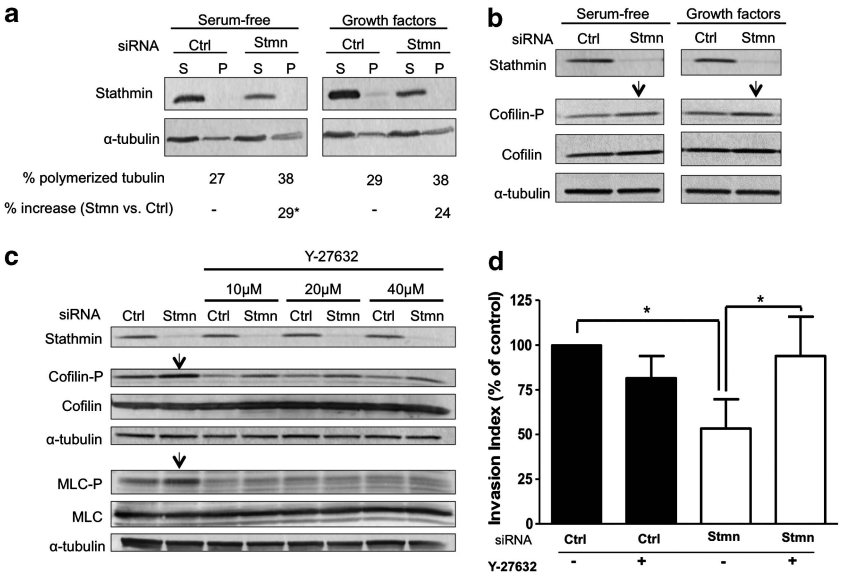

Figure 4. Stathmin suppression increases tubulin polymerization and the phosphorylation of cofilin and MLC. (**a**) Stathmin (Stmn) and control (Ctrl) siRNA-transfected BE(2)-C cells were serum-starved (serum-free), or serum-starved and then treated with growth factors (10% FCS/platelet-derived growth factor). Soluble (S) and polymerized (P) tubulin fractions were separated and α-tubulin and stathmin expression were analyzed by western blot ($n = 3$). The percentage of tubulin polymer levels and increase in these levels induced by stathmin suppression are shown below the representative α-tubulin blot (*$P < 0.05$). (**b**) Stmn and Ctrl siRNA-transfected BE(2)-C cells were serum-starved (serum-free) or serum-starved and then treated with growth factors (10% FCS/PDGF) for 15 min. The expression of stathmin, cofilin and phospho-cofilin (cofilin-P) were determined by western blot. Increased cofilin phosphorylation is indicated (*arrows*). (**c**) Stmn and Ctrl siRNA-transfected BE(2)-C cells were pretreated with 10–40 μmol/l of the ROCK inhibitor, Y-27632, for 1 h before incubation in serum-free media +/− Y-27632. The expression of stathmin, cofilin, cofilin-P, MLC and phospho-MLC were determined by western blot. Increases in cofilin and MLC phosphorylation are indicated (*arrows*). (**d**) Stmn siRNA-treated cells and Ctrl siRNA-treated cells were left untreated (minus symbol) or treated with 10 μmol/l Y-27632 (plus symbol) and subjected to transwell assays. Results are expressed as a percentage of untreated Ctrl siRNA cells (% of control). *$P < 0.05$.

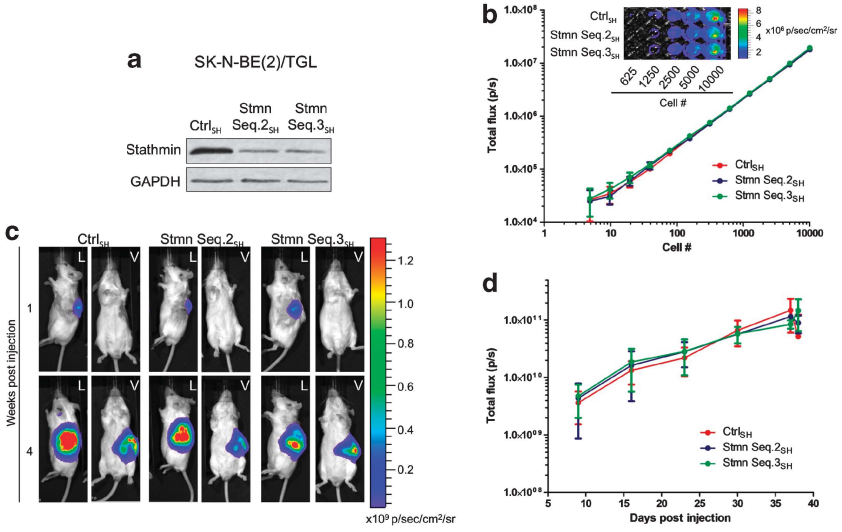

Figure 5. Stathmin does not influence neuroblastoma tumor burden. (**a**) Representative western blot showing stathmin expression in Ctrl$_{SH}$, Stmn Seq.2$_{SH}$ and Stmn Seq.3$_{SH}$ SK-N-BE(2)/TGL cells. Glyceraldehyde-3-phosphate dehydrogenase was used as a loading control. (**b**) Luciferase assays confirmed Ctrl$_{SH}$, Stmn Seq.2$_{SH}$ and Stmn Seq.3$_{SH}$ cells expressed similar levels of luciferase (total flux). A representative pseudocolor image of serially diluted cells is shown inset. (**c**) Representative pseudocolor images of Ctrl$_{SH}$, Stmn Seq.2$_{SH}$ and Stmn Seq.3$_{SH}$ mice 1 and 4 weeks after inoculation. Mice were imaged on their left lateral (L) and ventral (V) sides. (**d**) Increases in tumor burden (total flux) are observed over time for Ctrl$_{SH}$, Stmn Seq.2$_{SH}$ and Stmn Seq.3$_{SH}$ groups. Data represent the mean of at least 13 mice for each group ± s.e.m. (error bars).

siRNA-mediated ROCKI suppression did not reduce cofilin phosphorylation in stathmin-suppressed cells and a combination of ROCKI and ROCKII siRNA had no greater effect on reducing cofilin phosphorylation in stathmin-suppressed cells, compared with ROCKII siRNA alone (Supplementary Figures S3C, D). This data supports our results with H-1152, a chemical inhibitor that primarily targets ROCKII, and demonstrates that stathmin is regulating cofilin phosphorylation via ROCKII. Interestingly, the phosphorylation of MLC was also increased in stathmin-suppressed BE(2)-C cells and this increase was completely ablated

with 10 μmol/l Y-27632 (Figure 4c). This data indicates that while increases in MLC phosphorylation induced by stathmin suppression (and serum-starvation) solely depend on ROCK signaling, cofilin phosphorylation does not. Therefore, it appears that an alternate pathway also exists by which stathmin is regulating cofilin phosphorylation.

To determine whether stathmin's role in neuroblastoma cell invasion is also influenced by ROCK signaling, siRNA-transfected BE(2)-C cells were treated with ROCK inhibitors and subjected to invasion assays. Treatment of stathmin-suppressed cells with Y-27632 returned the level of cell invasion back to that of untreated control cells (invasion index (% of control) is 53.37 ± 7.3 for stathmin siRNA-treated cells vs 93.87 ± 9.84 for stathmin siRNA + Y-27632-treated cells; $P < 0.05$) (Figure 4d). Similarly, cell invasion of stathmin-suppressed cells was returned to levels of control cells upon treatment with H-1152 (Supplementary Figure S3B). Therefore, the reduction in cell invasion induced by stathmin suppression is reversed by ROCK inhibition.

Stathmin does not influence neuroblastoma tumor burden

To examine stathmin's role in neuroblastoma tumor growth and metastasis, stathmin shRNA/luciferase-expressing neuroblastoma cells (SK-N-BE(2)/TGL) were developed for use in a clinically relevant, orthotopic neuroblastoma mouse model. Stathmin was effectively suppressed by two individual shRNAs (targeting different regions of the stathmin gene), Stmn Seq.2_{SH} and Stmn Seq.3_{SH}, compared with controls ($Ctrl_{SH}$) as determined by western blotting (Figure 5a) and immunofluorescence microscopy (Supplementary Figure S4A). Bioluminescent imaging (BLI) confirmed that each of the shRNA-expressing SK-N-BE(2)/TGL cell populations expressed similar levels of luciferase (Figure 5b). Importantly, shRNA-mediated stathmin suppression inhibited the invasion of SK-N-BE(2)/TGL cells through Matrigel by 40% for Stmn Seq.2_{SH} (invasion index percentage of control $59.63\% \pm 3.72$, $P < 0.001$) and 44% for Stmn Seq.3_{SH} (invasion index percentage of control $56.03\% \pm 6.47$, $P < 0.001$) compared with controls (Supplementary Figure S4B). Similar to siRNA-transfected cells, stable suppression of stathmin did not influence anchorage-independent growth of SK-N-BE(2)/TGL cells (Supplementary Figure S4C).

To determine whether stathmin influenced engraftment or growth of neuroblastoma tumors, mice were orthotopically injected with shRNA-expressing SK-N-BE(2)/TGL cells, and tumor growth was measured each week using BLI. Stathmin suppression did not influence neuroblastoma tumor burden compared with controls (Figures 5c and d). Similarly, stathmin suppression did not significantly influence the growth of primary tumors compared with controls (Figure 6a), as demonstrated by measuring primary tumor volume (Figure 6b) and weight (Figure 6c). Stathmin suppression was maintained in the primary tumors, as confirmed at the mRNA level (stathmin mRNA was suppressed by 79% in Stmn Seq.2_{SH} ($P < 0.01$) and 82% in Stmn Seq.3_{SH} ($P < 0.05$) primary tumors compared with controls ($Ctrl_{SH}$)) (Figure 6d) and protein level, by western blotting (Figure 6e) and immunohistochemistry (IHC) (Figure 6f).

Stathmin regulates neuroblastoma metastasis

The movement of neuroblastoma cells from the primary tumor to the lungs represents hematogenous spread. We identified neuroblastoma metastases in the lungs of mice using BLI (Figure 7a) and IHC (Figure 7b). Notably, luciferase-expressing neuroblastoma tumors were present at different locations within a $Ctrl_{SH}$ lung (Supplementary Figure S5B, black arrowheads) but fewer were observed in a Stmn Seq.3_{SH} lung (Supplementary Figure S5D, black arrowheads). To determine whether stathmin suppression reduced neuroblastoma tumor burden in the lungs, bioluminescence from each mouse lung was quantified. Initially, 13 and 17 mice were orthotopically injected with Stmn Seq.2_{SH} cells and Stmn Seq.3_{SH} cells, respectively. However, as Stmn Seq.2_{SH} and Stmn Seq.3_{SH} cells had similar levels of stathmin suppression (Figure 5a), invasion (Supplementary Figure S4B), formed similarly sized tumors (Figures 6a-c), and there was no significant difference in neuroblastoma tumor burden in the lungs of these mice (median total flux of 9.13×10^6 for Stmn Seq.2_{SH} vs 3.69×10^7 for Stmn Seq.3_{SH}, $P = 0.315$) (Supplementary Figure S6), these groups were pooled (hereafter referred to as Stmn Seq.2/3_{SH}). Quantitation of mouse lung bioluminescence showed significantly reduced neuroblastoma tumor burden (71% reduction) in stathmin-suppressed mice compared with controls (median total flux of 2.17×10^7 for Stmn Seq.2/3_{SH} lungs vs 7.36×10^7 for $Ctrl_{SH}$ lungs, $P < 0.008$) (Figure 7c). This data provides the first evidence that stathmin suppression can significantly reduce the ability of neuroblastoma cells to metastasize *in vivo*.

DISCUSSION

Overexpression of stathmin in many cancers correlates with metastatic disease and a poor clinical outcome.[10,11,13,22–24] Despite this clinical correlation, studies addressing stathmin's contribution to metastasis *in vivo* have been limited. This is the first study to show that suppressing stathmin expression in neuroblastoma cells influenced ROCK signaling and reduced metastasis (hematogenous spread) in a clinically relevant animal model.

Suppression of stathmin decreased chemotactic migration and invasion and altered the cytoskeleton of neuroblastoma cells. These changes are likely to be mediated by stathmin's effect on the ROCK signaling pathway, as evidenced by increased cofilin and MLC phosphorylation in stathmin-suppressed cells. Inhibition of the ROCK pathway with Y-27632 (ROCKI and ROCKII inhibitor) or H-1152 (ROCKII inhibitor) in stathmin-suppressed cells returned cofilin phosphorylation back to that of untreated controls and importantly, reverted the invasion phenotype. This suggests that stathmin's regulation of cofilin phosphorylation may have a major role in neuroblastoma cell invasion. Indeed, Scott *et al.*[25] have proposed that the cycling of cofilin between inactive (phosphorylated) and active (dephosphorylated) states is a "key determinant of invasive and metastatic potential" in cancer cells. Specific targeting of ROCK using siRNA revealed that ROCKII (and not ROCKI) was mediating stathmin's effects on cofilin phosphorylation. However, stathmin's regulation of cofilin phosphorylation may include alternate signaling pathways as no difference in the expression or phosphorylation of LIM kinase 1 and LIM kinase 2,[26] or paxillin (downstream targets of ROCK signaling) were observed in stathmin-suppressed neuroblastoma cells (Supplementary Figures S7A and B). Independent of ROCK signaling, stathmin may influence cofilin activity indirectly through the microtubule network. Previous studies have shown that alterations in microtubule stability alter cofilin expression and phosphorylation in various cell types.[27–29] These affects are mediated via the RhoGTPase signaling pathways, of which stathmin is a key downstream target.[9,28,30–32]

Cancer cells utilize different modes of motility to invade and metastasize.[33] Our *in vitro* data clearly demonstrates that stathmin is influencing ROCK signaling in neuroblastoma cells; a pathway that facilitates ameboid (rounded cell morphology) motility. Activation of ROCK is also thought to inhibit mesenchymal (elongated-shape) motility, which requires proteolysis-mediated degradation of the surrounding extracellular matrix.[33] We have demonstrated that stathmin suppression activates ROCK signaling (as evidenced by increased cofilin and MLC phosphorylation) and that stathmin's regulation of cell invasion is mediated via ROCK. We therefore hypothesize that stathmin promotes a mode of motility (ameboid/mesenchymal) that neuroblastoma cells require to invade and metastasize. Interestingly, Belletti *et al.*[9,34] have demonstrated that direct interactions between $p27^{kip1}$ and stathmin mediate sarcoma cell invasion and that increased

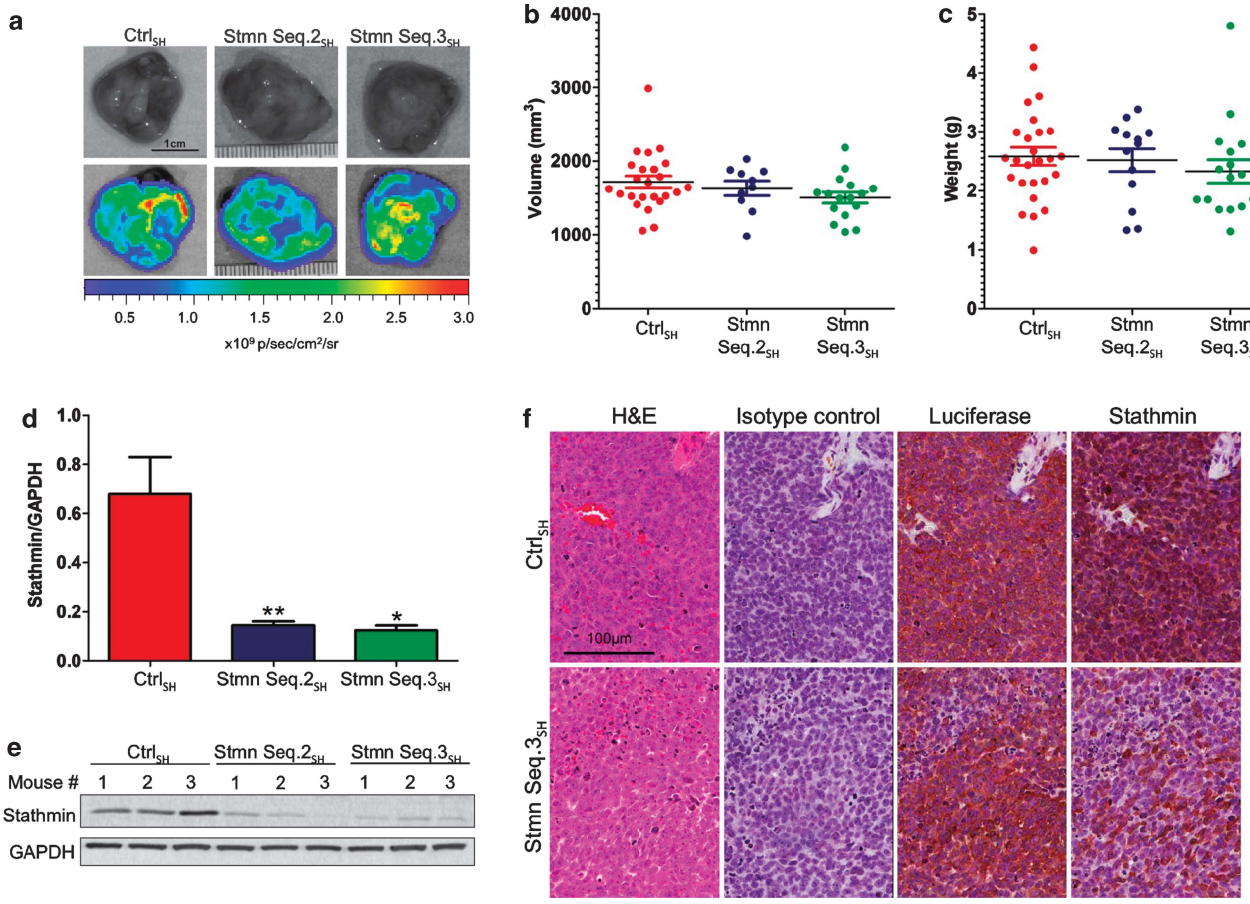

Figure 6. Stathmin does not influence neuroblastoma tumor growth. (**a**) Representative gray scale (top images) and pseudocolor (lower images) luminescent images of Ctrl$_{SH}$, Stmn Seq.2$_{SH}$ and Stmn Seq.3$_{SH}$ primary tumors. Graphs show primary tumor volumes (**b**) and weights (**c**). Data represent the mean of at least 10 primary tumors for each group ± s.e.m. (error bars). (**d**) Stathmin mRNA levels in Ctrl$_{SH}$, Stmn Seq.2$_{SH}$ and Stmn Seq.3$_{SH}$ primary tumors. (**e**) Representative western blot showing stathmin expression in three individual Ctrl$_{SH}$, Stmn Seq.2$_{SH}$ and Stmn Seq.3$_{SH}$ primary tumors. (**f**) Immunostaining of Ctrl$_{SH}$ and Stmn Seq.3$_{SH}$ primary tumors. Tumor cells were confirmed by hematoxylin and eosin (H&E) and luciferase staining, and stathmin immunostaining confirmed stathmin suppression in the Stmn Seq.3$_{SH}$ primary tumor compared with Ctrl$_{SH}$.

stathmin activity (that induced microtubule depolymerization) promoted ameboid-like cell invasion *in vitro* and higher metastatic potential *in vivo*. Studies to elucidate the mode of motility that stathmin regulates in neuroblastoma cells are currently underway in our laboratory.

Our *in vitro* data strongly supported a role for stathmin in neuroblastoma metastasis. Therefore, a clinically-relevant orthotopic mouse model was used to investigate stathmin's contribution to neuroblastoma metastasis. This model mimics human neuroblastoma development as reflected by the involvement of local organs, regional lymph nodes and distant sites (including the lungs).[35–37] In some animals, BLI and IHC detected neuroblastoma tumors on the surface of organs such as the liver, kidneys and spleen that were in close proximity to the primary tumor (data not shown). These tumors potentially arose from direct contact with the primary tumor or had occurred via loco-regional spread. However, for this study we focused on systemically spread metastases, such as those found in the lungs, as in patients they confer an extremely poor prognosis and are associated with other unfavorable features such as adrenal primary tumors, elevated lactate dehydrogenase and *MYCN* amplification.[4] In this model the lungs are separated from the primary tumor (injection site in fat pad above kidney) by the diaphragm and therefore any metastases found in this organ would be a direct result of hematogenous spread. Using BLI and IHC, we confirmed the presence of neuroblastoma cells in the lungs of mice. Importantly, quantitation of mouse lung bioluminescence demonstrated that stathmin suppression significantly inhibited the systemic spread of neuroblastoma cells *in vivo*.

In conclusion, this study has provided the first direct evidence that suppressing stathmin expression in neuroblastoma cells influences ROCK signaling and reduces metastasis in a clinically relevant orthotopic mouse model. These findings highlight stathmin as a potential therapeutic target for the treatment of neuroblastoma.

MATERIALS AND METHODS

Cell culture

Human neuroblastoma SK-N-BE(2) (obtained from Dr Sylvain Baruchel, The Hospital for Sick Children, Toronto, ON, Canada), BE(2)-C and SH-SY5Y cell lines (obtained from Dr June Biedler, Fordham University, NY, USA) were maintained in 10% fetal calf serum (FCS)/Dulbecco's Modified Eagle's Medium (DMEM) at 37°C/5% CO_2. Cells were validated by short tandem repeat profiling (CellBank Australia, Westmead, New South Wales, Australia) and were routinely screened and found to be free of mycoplasma.

siRNA transfections

Cells were transfected with 5 nmol/l STMN1 (Stmn), 50 nmol/l ROCKI (RI) or ROCKII (RII), or equivalent concentrations of non-targeting pool (Ctrl) ON-

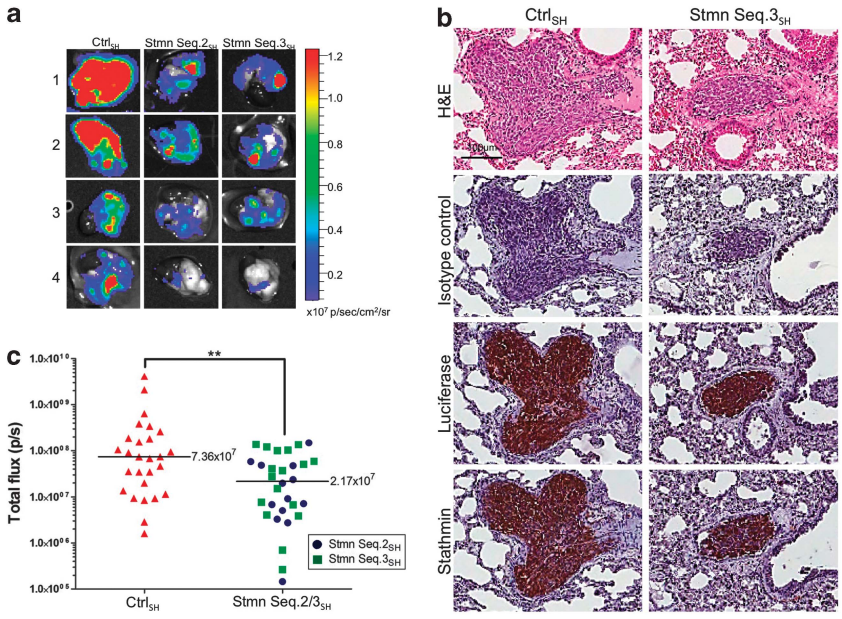

Figure 7. Stathmin suppression reduces neuroblastoma lung metastasis. (**a**) Representative pseudocolor luminescent images of Ctrl$_{SH}$, Stmn Seq.2$_{SH}$ and Stmn Seq.3$_{SH}$ mouse lungs. (**b**) Immunostaining of metastatic neuroblastoma tumors in the lungs of Ctrl$_{SH}$ and Stmn Seq.3$_{SH}$ mice. Tumor cells were confirmed by H&E and luciferase staining. Metastatic tumors were also positive for stathmin. (**c**) Neuroblastoma tumor burden in Ctrl$_{SH}$ (red triangles) and Stmn Seq.2/3$_{SH}$ (mice pooled from Stmn Seq.2$_{SH}$ (blue dots) and Stmn Seq.3$_{SH}$ (green squares)) lungs were quantified by measuring the total flux (photons/sec) from each lung ($n \geqslant 27$ for each group). Each dot represents one lung and the bar represents the median total flux for each group. The median total flux value is displayed to the right of the bar. $^{**}P < 0.008$.

TARGETplus SMARTpool siRNA (Thermo Fisher Scientific, Waltham, MA, USA) using Lipofectamine 2000 (Invitrogen, Carlsbad, CA, USA) as the delivery vehicle. Cells were double-transfected with STMN1 siRNA (24 h apart) to maximize and prolong stathmin suppression.

Real-time quantitative PCR (qPCR)

RNA was isolated as previously described[38] and reverse transcription and qPCR was performed using the Quantitect SYBR green PCR kit and the STMN1_1_SG QuantiTect Primer Assay (Qiagen, Melbourne, Victoria, Australia) using an Applied Biosystems 7500 PCR system. Stathmin mRNA expression was normalized to β2-microglobulin or glyceraldehyde-3-phosphate dehydrogenase (Quantitect primer assays, Qiagen).

Western blotting

Cells and frozen tumor tissue were solubilized in radio-immunoprecipitation assay buffer containing protease and phosphatase inhibitors (Roche Diagnostics Australia, Castle Hill, New South Wales, Australia). Total cellular proteins (10–30 μg) were resolved on 15% SDS–polyacrylamide gel electrophoresis or Criterion 4–20% Tris-HCl gels (Bio-Rad Laboratories, Hercules, CA, USA) and electro transferred to nitrocellulose membrane. Proteins were detected using the following antibodies; stathmin/metablastin (BD Biosciences, Franklin Lakes, NJ, USA), superior cervical ganglion-10 protein (generous gift provided by Dr Dominic Chi Hiung Ng, University of Melbourne), LIMK1 and LIMK2 (generous gifts provided by Dr Ora Bernard, St Vincent's Institute of Medical Research), cofilin (Abcam, Cambridge, UK), myosin (light chains) (Sigma-Aldrich, St Louis, MO, USA), paxillin (BD Biosciences), ROCKI and ROCKII antibodies (Cell Signaling Technology). Phosphorylation of LIMK1 (T508), LIMK2 (T505), cofilin (S3) and MLC (S20) were detected using Abcam antibodies and paxillin (Y118) with an Invitrogen antibody. Glyceraldehyde-3-phosphate dehydrogenase (Abcam) and α-tubulin (clone DM1A) (Sigma-Aldrich) were used as loading controls. Primary antibodies were detected using horseradish peroxidase–linked polyclonal antibodies (GE Healthcare Life Sciences, Uppsala, Sweden) and membranes developed using ECL Plus Western blotting reagent (GE Healthcare). Signal was detected with a Typhoon 9410 laser scanner (GE Healthcare) or X-ray developer (Okamoto, Japan).

Protein phosphorylation

Cells were serum-starved for 2 h, treated with growth factor medium (10% FCS or 10% FCS plus 25 ng/ml human recombinant platelet-derived growth factor -BB (Sigma-Aldrich) in DMEM) for the indicated time points, harvested in ice-cold phosphate-buffered saline (PBS) and prepared for western blotting. Of note, treatment of cells with 10% FCS or 10% FCS/platelet-derived growth factor did not alter the outcome of protein phosphorylation and conditions used are indicated in figure legends. For ROCK inhibitor experiments, cells were pretreated for 1 h with the indicated concentrations of Y-27632 (Sigma-Aldrich) or H-1152 (Merck KGaA, Darmstadt, Germany) in normal cell culture medium, incubated with equivalent concentrations of the ROCK inhibitors in serum-free DMEM for 2 h and then harvested, as described above. For ROCK siRNA experiments, cells were harvested following incubation in serum-free DMEM for 2 h.

Cell proliferation

Following siRNA transfection (24 h), cells were seeded into 96-well plates, and cellular metabolic activity was measured using resazurin solution (597 μmol resazurin, 67 μmol methylene blue, 1 μmol potassium hexacyanoferrate (III), 1 μmol potassium hexacyanoferrate (II) trihydrate in PBS) and fluorescence was detected using a Victor2 plate reader (Perkin Elmer, Waltham, MA, USA).

Soft agar assays

Cells were grown in soft agar for 2 weeks, as described.[38] Individual colonies were counted and photographed using the Axiovert 200 M microscope (Zeiss, Oberkochen, Germany) coupled to an AxioCamMR3 camera driven by the Axio Vision software (Zeiss). Results are expressed as percentage colony formation ((number of colonies formed/total number of cells seeded) × 100).

Migration/invasion assays

Following siRNA transfection (24 h), cells were incubated in serum-free DMEM for 2 h. For experiments using the ROCK inhibitors, cells were pretreated with 10 μmol/l Y-27632 or H-1152 for 1 h before incubation in serum-free DMEM (containing equivalent concentrations of the ROCK inhibitors) for 2 h. The underside of 8 μm polyethylene terephthalate 24-well migration inserts or 8 μm BD Biocoat BD Matrigel 24-well invasion chambers (BD Biosciences) were coated with 10 μg per ml collagen IV (BD Biosciences) and incubated at room temperature for 1 h. Cells were harvested, resuspended in serum-free DMEM and seeded into the top chamber. The lower chamber contained 10% FCS + 25 ng per ml platelet-derived growth factor (diluted in DMEM). For the ROCK inhibitor

experiments, these compounds were added to the top and bottom chambers at a final concentration of 10 μmol/l for the duration of the experiment. After seeding, cells were incubated for 24–48 h at 37 °C before fixing inserts with methanol and staining with May–Grunwald (Sigma-Aldrich) and Giemsa (Sigma-Aldrich), as previously described.[39] Dry membranes were mounted on glass slides and 15 random images were taken of each (top and bottom surfaces) using a ×20 objective. Results are expressed as a migration or invasion index ((number of cells on undersurface of membrane divided by total number of cells on both surfaces of the membrane) × 100) or an invasion index (% of control).

Microscopy

Cells were imaged using the Axiovert S100 inverted phase-contrast microscope (Zeiss) equipped with a SPOT RT Slider CCD scientific digital camera system driven by SPOT Basic software (Diagnostic Instruments Inc., Sterling Heights, MI, USA). For immunofluorescence microscopy, cells were seeded in four-well Nunc Lab-Tek chamber slides (Thermo Fisher Scientific) and incubated at 37 °C for 24 h. Cells were fixed in ice-cold methanol or 4% paraformaldehyde. Paraformaldehyde -fixed cells were permeabilized with 1% Triton X/PBS. Fixed cells were blocked in 10% FCS/PBS and incubated with α-tubulin and stathmin antibodies (as described for western blotting). Primary antibodies were detected using Alexa Fluor 488 goat anti-mouse ImmunoglobulinG (Invitrogen). Actin filaments were stained with Alexa Fluor 568 Phalloidin (Invitrogen). Slides were mounted using VECTASHIELD mounting medium with 4′,6-diamidino-2-phenylindole (Vector Laboratories, Burlingame, CA, USA). Cytoskeletal structures were then visualized and imaged using an Olympus FluoView FV1000 confocal microscope with a ×63 1.35 numerical aperture oil objective.

Tubulin polymerization assay

Following siRNA transfection (48 h), cells were serum-starved in DMEM for 2 h or serum-starved and treated with 10% FCS + 25 ng per ml platelet-derived growth factor for 1 h. Fractions of polymerized (insoluble) and depolymerized (soluble) tubulin were extracted from cells, as described previously.[17] Tubulin fractions (soluble 'S' and polymerized 'P') were detected by western blot using total α-tubulin antibody. The levels of polymerized tubulin were quantified by densitometry and the percentage of polymerized tubulin was calculated as follows (('P'/ 'P' + soluble 'S') × 100).

Short hairpin RNA/luciferase-expressing neuroblastoma cells

The SFG-$_{NES}$ (SFG-Ntp backbone with nuclear export signal) TGL triple-modality reporter construct, harboring the herpes virus 1 thymidine kinase gene, Aequorea victoria green fluorescent protein gene and the *Photinus pyralis* (firefly) luciferase gene,[40] was retrovirally delivered into SK-N-BE(2) cells (hereafter, designated SK-N-BE(2)/TGL cells). A high green fluorescent protein-expressing cell population was selected by fluorescence-activated cell sorting. These cells were stably transfected with two individual stathmin short hairpin RNA HuSH retroviral silencing plasmids (designated Stmn Seq.2$_{SH}$ and Stmn Seq.3 $_{SH}$) targeting different regions of the stathmin gene or a HuSH noneffective retroviral silencing plasmid (Ctrl$_{SH}$) (Origene Technologies Inc., Rockville, MD, USA). The short hairpin RNA sequences are as follows; 5′-GCACTACCAGAGCTAACTCAGATAGTACT-3′ (Ctrl$_{SH}$), 5′-TCTTACCAGATGCTACTGGACTTGAATGG-3′ (Stmn Seq.2$_{SH}$), 5′-GAATACACTGCCTGTCGCTTGTCTTCTAT-3′ (Stmn Seq.3$_{SH}$).

Orthotopic neuroblastoma mouse model

Short hairpin RNA-expressing SK-N-BE(2)/TGL cells (2×10^6 resuspended in 20 μl Cultrex basement membrane extract (Trevigen Inc., Gaithersburg, MD, USA)) were orthotopically injected into 8.5 week-old male severe combined immunodeficiency-Beige mice, as previously described.[36] Mice with obvious leakage from the injection site were not included in the study. The peritoneum was closed with Safil 5/0 absorbable sutures (B. Braun Australia, Bella Vista, Sydney, New South Wales, Australia) and the skin layer with Reflex 7 mm stainless steel wound clips (Fine Science Tools Inc., North Vancouver, BC, Canada). Mice were euthanized when the tumor reached 1500 mm^3 (by palpation), 38 days post-injection or if the mice were of ill thrift. Tumor size was measured in weight and volume (mm^3) using the formula: volume = (length × width × depth)/2. All animal experiments were approved by the Animal Ethics Committee, University of New South Wales (ACEC no.: 10/114A).

In vitro luciferase assays

D-luciferin potassium salt (Gold Biotechnology, St Louis, MO, USA) was reconstituted in Dulbecco's PBS (Life Technologies, Melbourne, Victoria, Australia). Cells were serially diluted into 96-well plates, incubated with luciferin (3 h) and imaged using the IVIS Imaging System (Xenogen, Alameda, CA, USA). Bioluminescent signal was analyzed using the LIVINGIMAGE software (Xenogen) and photon emission (measured as total flux (photons/second)) was determined using the region of interest method as described in the Caliper Life Sciences manual (Caliper Life Sciences, Hopkinton, MA, USA).

In vivo and *ex vivo* luciferase detection

Luciferase-expressing neuroblastoma cells were visualized *in vivo* via intraperitoneal injection of 150 mg per kg D-luciferin. Animals were anaesthetized, placed inside the IVIS Imaging System specimen chamber and imaged 10 min after substrate injection. Mice with obvious leakage from the injection site (imaged 1 day after surgery) were killed and eliminated from the study. Remaining mice were imaged 9 days post injection, every week thereafter and on the day of killing. For *ex vivo* imaging, 150 mg per kg D-luciferin was injected intraperitoneal before necropsy. Animals were killed and their tumor and organs collected and covered with D-luciferin. Bioluminescent images of the mice and organs were digitized and electronically displayed as a pseudocolor overlay onto a gray scale image on the LIVINGIMAGE software. Colored scale bars on figures indicate the amount of bioluminescence as measured in photons/second/centimeter squared/steradian (p/sec/cm^2/sr). Bioluminescence signal was then quantified from the left lateral side of the live animal and the organs post killing using the region of interest method. To determine background bioluminescence, two naïve mice and their organs were imaged as described above. The mean bioluminescent signal (total flux) from the left lateral side of the naïve mice was 511700 photons/sec and 10478 photons/sec for the lungs. These values were subtracted from the signal obtained from similarly sized region of interests from tumor bearing mice.

Immunohistochemistry (IHC)

Tissue sections were incubated with rabbit polyclonal antibodies against luciferase (Fitzgerald, Acton, MA, USA) and stathmin (Abcam). 3,3′-Diaminobenzidine was used as a substrate for the peroxidase reaction and hematoxylin as the counterstain. To ensure antibody specificity, extra slides were incubated with rabbit ImmunoglobulinG control antibody at a concentration equivalent to the primary antibodies. Slides were scanned using an Aperio ScanScope XT Slide Scanner (Aperio, Vista, CA, USA). Images were analyzed using the ImageScope software (Aperio).

Statistical analyses

Statistical analyses were performed using the GraphPad Prism program. Results are expressed as means of at least three independent experiments ± s.e.m. (error bars). Unpaired two-tailed Student's *t*-tests were used to determine the statistical differences between various experimental and control groups, with $P<0.05$ considered statistically significant. The bioluminescent signal from mouse lungs were compared using the Mann–Whitney *U*-test, where $P<0.05$ was considered statistically significant.

CONFLICT OF INTEREST

The authors declare no conflict of interest.

ACKNOWLEDGEMENTS

We thank Dr Vladimir Ponomarev (Memorial Sloan Kettering Cancer Center) for kindly providing the TGL reporter vector, Dr Michael Shum and Dr Toby Trahair for helpful discussions and Zillan Neiron for technical assistance. Biological Resources Imaging Laboratory and the Biomedical Imaging Facility, Mark Wainwright Analytical Center, University of New South Wales. This study was financially supported by: Children's Cancer Institute Australia for Medical Research, which is affiliated with the University of New South Wales and the Sydney Children's Hospital. Funding from the Anthony Rothe Memorial Trust (F Byrne, The Anthony Rothe Scholarship) and grants from the National Health and Medical Research Council (NHMRC) (M Kavallaris and J McCarroll), Cancer Council New South Wales Program Grant (M Kavallaris), Cure Cancer Australia Foundation Grant (J McCarroll), Cancer Institute New South Wales Early Career Development Fellowship (J McCarroll, J Fletcher), NHMRC Career

Development Fellowship (P Phillips) and an NHMRC Senior Research Fellowship (M Kavallaris).

REFERENCES

1 Gutierrez JC, Fischer AC, Sola JE, Perez EA, Koniaris LG. Markedly improving survival of neuroblastoma: a 30-year analysis of 1646 patients. *Pediatr Surg Int* 2007; **23**: 637–646.
2 Ara T, DeClerck YA. Mechanisms of invasion and metastasis in human neuroblastoma. *Cancer Metastasis Rev* 2006; **25**: 645–657.
3 DuBois SG, Kalika Y, Lukens JN, Brodeur GM, Seeger RC, Atkinson JB *et al.* Metastatic sites in stage IV and IVS neuroblastoma correlate with age, tumor biology, and survival. *J Pediatr Hematol Oncol* 1999; **21**: 181–189.
4 DuBois SG, London WB, Zhang Y, Matthay KK, Monclair T, Ambros PF *et al.* Lung metastases in neuroblastoma at initial diagnosis: a report from the International Neuroblastoma Risk Group (INRG) project. *Pediatr Blood Cancer* 2008; **51**: 589–592.
5 Insall RH, Machesky LM. Actin dynamics at the leading edge: from simple machinery to complex networks. *Dev Cell* 2009; **17**: 310–322.
6 Torka R, Thuma F, Herzog V, Kirfel G. ROCK signaling mediates the adoption of different modes of migration and invasion in human mammary epithelial tumor cells. *Exp Cell Res* 2006; **312**: 3857–3871.
7 Kadir S, Astin JW, Tahtamouni L, Martin P, Nobes CD. Microtubule remodelling is required for the front-rear polarity switch during contact inhibition of locomotion. *J Cell Sci* 2011; **124**: 2642–2653.
8 Curmi PA, Gavet O, Charbaut E, Ozon S, Lachkar-Colmerauer S, Manceau V *et al.* Stathmin and its phosphoprotein family: general properties, biochemical and functional interaction with tubulin. *Cell Struct Funct* 1999; **24**: 345–357.
9 Belletti B, Nicoloso MS, Schiappacassi M, Berton S, Lovat F, Wolf K *et al.* Stathmin activity influences sarcoma cell shape, motility, and metastatic potential. *Mol Biol Cell* 2008; **19**: 2003–2013.
10 Hsieh SY, Huang SF, Yu MC, Yeh TS, Chen TC, Lin YJ *et al.* Stathmin1 overexpression associated with polyploidy, tumor-cell invasion, early recurrence, and poor prognosis in human hepatoma. *Mol Carcinog* 2010; **49**: 476–487.
11 Jeon TY, Han ME, Lee YW, Lee YS, Kim GH, Song GA *et al.* Overexpression of stathmin1 in the diffuse type of gastric cancer and its roles in proliferation and migration of gastric cancer cells. *Br J Cancer* 2010; **102**: 710–718.
12 Saal LH, Johansson P, Holm K, Gruvberger-Saal SK, She QB, Maurer M *et al.* Poor prognosis in carcinoma is associated with a gene expression signature of aberrant PTEN tumor suppressor pathway activity. *Proc Natl Acad Sci USA* 2007; **104**: 7564–7569.
13 Trovik J, Wik E, Stefansson IM, Marcickiewicz J, Tingulstad S, Staff AC *et al.* Stathmin overexpression identifies high-risk patients and lymph node metastasis in endometrial cancer. *Clin Cancer Res* 2011; **17**: 3368–3377.
14 Sadow PM, Rumilla KM, Erickson LA, Lloyd RV. Stathmin expression in pheochromocytomas, paragangliomas, and in other endocrine tumors. *Endocr Pathol* 2008; **19**: 97–103.
15 Hailat N, Strahler J, Melhem R, Zhu XX, Brodeur G, Seeger RC *et al.* N-myc gene amplification in neuroblastoma is associated with altered phosphorylation of a proliferation related polypeptide (Op18). *Oncogene* 1990; **5**: 1615–1618.
16 Campostrini N, Pascali J, Hamdan M, Astner H, Marimpietri D, Pastorino F *et al.* Proteomic analysis of an orthotopic neuroblastoma xenograft animal model. *J Chromatogr B Analyt Technol Biomed Life Sci* 2004; **808**: 279–286.
17 Don S, Verrills NM, Liaw TY, Liu ML, Norris MD, Haber M *et al.* Neuronal-associated microtubule proteins class III beta-tubulin and MAP2c in neuroblastoma: role in resistance to microtubule-targeted drugs. *Mol Cancer Ther* 2004; **3**: 1137–1146.
18 Yamaguchi H, Condeelis J. Regulation of the actin cytoskeleton in cancer cell migration and invasion. *Biochim Biophys Acta* 2007; **1773**: 642–652.
19 Gutjahr MC, Rossy J, Niggli V. Role of Rho, Rac, and Rho-kinase in phosphorylation of myosin light chain, development of polarity, and spontaneous migration of Walker 256 carcinosarcoma cells. *Exp Cell Res* 2005; **308**: 422–438.
20 Narumiya S, Ishizaki T, Uehata M. Use and properties of ROCK-specific inhibitor Y-27632. *Methods Enzymol* 2000; **325**: 273–284.
21 Tamura M, Nakao H, Yoshizaki H, Shiratsuchi M, Shigyo H, Yamada H *et al.* Development of specific Rho-kinase inhibitors and their clinical application. *Biochim Biophys Acta* 2005; **1754**: 245–252.
22 Salvesen HB, Carter SL, Mannelqvist M, Dutt A, Getz G, Stefansson IM *et al.* Integrated genomic profiling of endometrial carcinoma associates aggressive tumors with indicators of PI3 kinase activation. *Proc Natl Acad Sci USA* 2009; **106**: 4834–4839.
23 Singer S, Malz M, Herpel E, Warth A, Bissinger M, Keith M *et al.* Coordinated expression of stathmin family members by far upstream sequence element-binding protein-1 increases motility in non-small cell lung cancer. *Cancer Res* 2009; **69**: 2234–2243.
24 Yuan RH, Jeng YM, Chen HL, Lai PL, Pan HW, Hsieh FJ *et al.* Stathmin overexpression cooperates with p53 mutation and osteopontin overexpression, and is associated with tumour progression, early recurrence, and poor prognosis in hepatocellular carcinoma. *J Pathol* 2006; **209**: 549–558.
25 Scott RW, Hooper S, Crighton D, Li A, Konig I, Munro J *et al.* LIM kinases are required for invasive path generation by tumor and tumor-associated stromal cells. *J Cell Biol* 2010; **191**: 169–185.
26 Bernard O. Lim kinases, regulators of actin dynamics. *Int J Biochem Cell Biol* 2007; **39**: 1071–1076.
27 Balasubramani M, Nakao C, Uechi GT, Cardamone J, Kamath K, Leslie KL *et al.* Characterization and detection of cellular and proteomic alterations in stable stathmin-overexpressing, taxol-resistant BT549 breast cancer cells using offgel IEF/PAGE difference gel electrophoresis. *Mutat Res* 2011; **722**: 154–164.
28 Belletti B, Pellizzari I, Berton S, Fabris L, Wolf K, Lovat F *et al.* p27kip1 controls cell morphology and motility by regulating microtubule-dependent lipid raft recycling. *Mol Cell Biol* 2010; **30**: 2229–2240.
29 Takesono A, Heasman SJ, Wojciak-Stothard B, Garg R, Ridley AJ. Microtubules regulate migratory polarity through Rho/ROCK signaling in T cells. *PLoS ONE* 2010; **5**: e8774.
30 Wittmann T, Waterman-Storer CM. Cell motility: can Rho GTPases and microtubules point the way? *J Cell Sci* 2001; **114**: 3795–3803.
31 Takahashi K, Suzuki K. Membrane transport of WAVE2 and lamellipodia formation require Pak1 that mediates phosphorylation and recruitment of stathmin/Op18 to Pak1-WAVE2-kinesin complex. *Cell Signal* 2009; **21**: 695–703.
32 Takahashi K, Tanaka T, Suzuki K. Directional control of WAVE2 membrane targeting by EB1 and phosphatidylinositol 3,4,5-triphosphate. *Cell Signal* 2010; **22**: 510–518.
33 Yilmaz M, Christofori G. Mechanisms of motility in metastasizing cells. *Mol Cancer Res* 2010; **8**: 629–642.
34 Baldassarre G, Belletti B, Nicoloso MS, Schiappacassi M, Vecchione A, Spessotto P *et al.* p27(Kip1)-stathmin interaction influences sarcoma cell migration and invasion. *Cancer Cell* 2005; **7**: 51–63.
35 Nevo I, Sagi-Assif O, Edry Botzer L, Amar D, Maman S, Kariv N *et al.* Generation and characterization of novel local and metastatic human neuroblastoma variants. *Neoplasia* 2008; **10**: 816–827.
36 Khanna C, Jaboin JJ, Drakos E, Tsokos M, Thiele CJ. Biologically relevant orthotopic neuroblastoma xenograft models: primary adrenal tumor growth and spontaneous distant metastasis. *In Vivo* 2002; **16**: 77–85.
37 Henriksson KC, Almgren MA, Thurlow R, Varki NM, Chang CL. A fluorescent orthotopic mouse model for reliable measurement and genetic modulation of human neuroblastoma metastasis. *Clin Exp Metastasis* 2004; **21**: 563–570.
38 McCarroll JA, Gan PP, Liu M, Kavallaris M. betaIII-tubulin is a multifunctional protein involved in drug sensitivity and tumorigenesis in non-small cell lung cancer. *Cancer Res* 2010; **70**: 4995–5003.
39 Phillips PA, Wu MJ, Kumar RK, Doherty E, McCarroll JA, Park S *et al.* Cell migration: a novel aspect of pancreatic stellate cell biology. *Gut* 2003; **52**: 677–682.
40 Ponomarev V, Doubrovin M, Serganova I, Vider J, Shavrin A, Beresten T *et al.* A novel triple-modality reporter gene for whole-body fluorescent, bioluminescent, and nuclear noninvasive imaging. *Eur J Nucl Med Mol Imaging* 2004; **31**: 740–751.

Supplementary Information accompanies the paper on the Oncogene website (http://www.nature.com/onc)